Journal of Sound and Vibration (1997) **207**(3), 287–299

STABILITY ANALYSIS FOR THE DYNAMIC DESIGN OF ROTORS

N. KHADER†

Department of Mechanical Engineering, University of Science and Technology, P.O. Box 3030, *Irbid*-22110, *Jordan*

(*Received* 16 *September* 1996, *and in final form* 25 *April* 1997)

The dynamic behaviour of a cantilever flexible shaft, carrying a rigid disk at its free end is presented. The stability of the rotating shaft–disk system, subjected to periodic follower axial force and end moment is investigated. Due to the periodic nature of the external loads, the governing equations of motion contain periodic coefficients, which cannot be solved by the available classical eigenvalue routines. Floquet theory is used along with the Runge–Kutta method with Gill coefficients to calculate the transition matrix, whose eigenvalues provide the desired information about system stability. The effect of various system parameters on the calculated stability boundaries is examined. Such examination includes rotor speed, damping available in the system and associated with both translation and tilting of the shaft cross-sections, torque to damping ratio, and axial force to end torque ratio.

INTRODUCTION

The improved reliability of rotors has been, and still is a primary concern for designers and researchers, who have over the years examined their dynamic behaviour in order to explore all possible means to improve their performance and to achieve the desired design, which has the highest reliability at minimum cost. Examples of such rotors are bladed disks found in fans, compressors and turbines, impellers found in compressors and pumps, as well as aircraft propeller drives and helicopter rotors. Due to pressure difference across the bladed disk or the impeller, they will be subject to a resultant axial force. Fluid resistance, however, will generate a load torque, which can be positive or negative. When the shaft in a gas turbine drives the bladed disk of a compressor, it will do work on the fluid, and the torque is negative. A positive torque load, however, acts on turbine disk when the working fluid drives the bladed disk of the turbine. Flexibility of the supporting shaft will cause the bladed disk or impeller to move and tilt, and the axial force and torque produced, which are expected to be periodic due to rotation, will remain normal to the plane of the disk or impeller and tangential to the axis of the shaft. The dynamic stability of rotors subjected to periodic loads, has been a main concern of researchers for a long period of time. Several published works on the subject are listed in the book by Loewy and Piaruli [1]. More recent works which deal with further developments in the field are available. For example, Ishida *et al*. [2], studied the parametric resonance and the influence of rotor speed on the unstable regions of a shaft–disk system loaded by a sinusoidal axial force. Kar and Sujata [3] examined the parametric instability of a rotating uniform beam under pulsating axial force, and examined the effect of rotor speed on the dynamic

† This work was submitted for publication while the author was a visiting scholar at Concordia University, Montreal, Canada.

0022–460X/97/430287 + 13 $25.00/0/sv971104

instability regions for various combinations of free, hinged, guided, and clamped boundary conditions. Chen and Ku [4] employed the finite element method to study the dynamic stability of a shaft–disk system subjected to a periodic axial force, where the shaft was modelled as a Timoshenko beam, with shear deformation and rotary inertia taken into consideration. Sinha [5] used Galerkin's method to examine the dynamic stability of a viscoelastic shaft subject to a periodic axial force. In another work [6], he examined the dynamic stability of a Timoshenko beam subjected to a periodic sinusoidal axial force superimposed on a static axial component. Namachchivaya [7] considered the dynamic stability of rotating shafts under parametric excitation consisting of a combination of harmonic terms and stationary stochastic processes. The dynamic stability of shaft–disk system loaded by follower torque loads was also addressed by a number of researchers [8–13] as discussed by Khader [8], who considered the stability of a shaft–disk system loaded by a follower axial force and end torque. Aida *et al*. [14] examined the dynamic stability of structural members with a thin-walled cross-section subjected to a follower periodic axial force and torque.

The work presented here deals with the dynamic stability of shaft–disk systems loaded by a periodic follower axial force and end moment. Lagrange's equation along with the assumed mode method are employed to derive the governing equations of motion, which have periodic coefficients due to the periodic nature of the applied load. The resulting eigenvalue problem from such equations cannot be analysed by the available classical eigenvalue routines. A method based on Floquet theory is employed to discover all types of instabilities, where the Runge–Kutta method with Gill coefficients, proposed by Friedman and Hammond [15], is used for efficient numerical integration to calculate the transition matrix at the end of one period. The eigenvalues of the transition matrix are used to calculate the characteristic exponents of the system, whose real part is a measure of system stability. The stability boundaries for the shaft–disk system considered are presented, and the effect on these boundaries of damping, rotor speed, ratio of the applied force and end torque to the available damping, and ratio of the applied axial force to the applied end torque is evaluated.

2. EQUATIONS OF MOTION

The Lagrangian approach is used to derive the governing equations of motion for a cantilever shaft carrying a rigid disk at its free end, where the shaft–disk assembly is subjected to a periodic follower axial force and torque load. The kinetic energy T, potential energy U, dissipation function D, and the work of external loads W_e are written in terms of some time-dependent generalised co-ordinates with subsequent application of Lagrange's equation.

2.1. STRUCTURAL MODEL

The system considered consists of a flexible cantilever shaft, with a uniformly distributed mass m_s, polar and diametral mass moments of inertia I_{ps} and I_{ds} respectively, and bending rigidity $(EI)_s$, taken the same in the two principal directions. A rigid disk with mass M_d and polar and diametral mass moments of inertia I_{pd} and I_{dd}, respectively, is attached at the free end of the shaft. The position vector X for any arbitrary mass element of the non-rotating shaft–disk system is defined in the undeformed position by its spanwise Z, radial r, and angular θ_z positions. The centreline of the shaft is allowed to bend by $U_s(Z, t)$ and $V_s(Z, t)$ along the X- and Y- axes of a fixed-in-space co-ordinate system, which results in tilting of the shaft's cross-section by $\theta_{sX}(Z, t) = \partial V_s(Z, t)/\partial Z$ and $\theta_{sY}(Z, t) = \partial U_s(Z, t)/\partial Z$ about the same axes, respectively. Due to bending of the shaft's

centreline and tilting of its cross-section, the disk will have two rigid-body translations $U_d(t) = U_s(Z = \ell, t)$ and $V_d(t) = V_s(Z = \ell, t)$, and two rigid-body rotations $\theta_{dX}(Z, t) = \partial V_s(Z = \ell, t)/\partial Z$ and $\theta_{dY}(t) = \partial U_s(Z = \ell, t)/\partial Z$, along and about the X- and Y-axes, respectively. As the shaft rotates with a constant angular velocity ω_R, the disk and each shaft cross-section will rotate about an axis normal to their planes at an angle $\omega_R t$. The position vector for any disk $(dm)_d$ or shaft $(dm)_s$ element in the rotating and deformed position, is given in the non-rotating and attached-to-cross-section co-ordinate system $X_2 Y_2 Z_2$ by

$$\{X\} = \begin{Bmatrix} r\cos\psi \\ r\sin\psi \\ 0 \end{Bmatrix},$$

where $\psi = \theta_z + \omega_R t$. As shown in Figure 1, the $X_2 Y_2 Z_2$ co-ordinate system is related to the intermediate system $X_1 Y_1 Z_1$ by V_s, the displacement along the Y-axis, and the associated with it tilting, θ_{sX}. The intermediate co-ordinate system $X_1 Y_1 Z_1$ is related to the fixed-in-space system XYZ by Z, the spanwise position of the cross-section the displacement along the X-axis, U_s, and the associated with it tilting, θ_{sY}. Through the appropriate co-ordinate transformations, the position $\{X\}$ and velocity $\{\dot{X}\}$ vectors can be expressd in the fixed-in-space system as

$$\{X\} = \begin{Bmatrix} U + r\cos\psi\cos\theta_Y \\ V + r\sin\psi\cos\theta_X - r\cos\psi\sin\theta_Y\sin\theta_X \\ -r\sin\psi\sin\theta_X - r\cos\psi\sin\theta_Y\cos\theta_X \end{Bmatrix}, \tag{1}$$

$$\{\dot{X}\} = \dot{U}\{\partial X/\partial U\} + \dot{V}\{\partial X/\partial V\} + \dot{\theta}_X\{\partial X/\partial\theta_X\} + \dot{\theta}_Y\{\partial X/\partial\theta_Y\} + \dot{\psi}\{\partial X/\partial\psi\}. \tag{2}$$

Expressions for the kinetic energy T, potential energy U, dissipation function D, and work of external periodic non-conservative loads W_e are expressed in terms of the transverse bending components U_s and V_s of the shaft and the associated rotations of its cross-section, U_s' and V_s' as

$$T = \frac{1}{2}\int_{Vol}(\{\dot{X}\}^{\mathrm{T}}\cdot\{\dot{X}\}\,\mathrm{d}m)_s + \frac{1}{2}\int_{Vol}(\{\dot{X}\}^{\mathrm{T}}\cdot\{\dot{X}\}\,\mathrm{d}m)_d \tag{3}$$

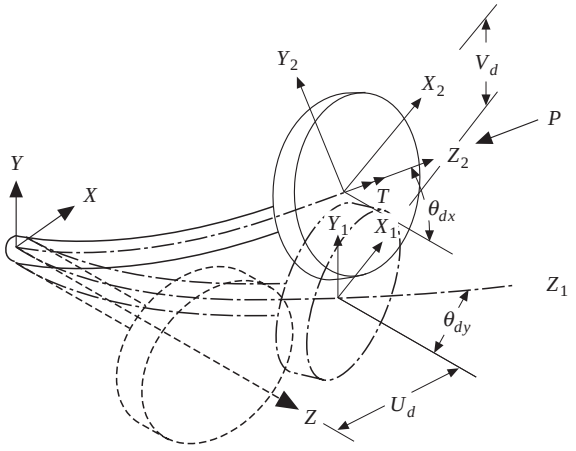

Figure 1. The shaft–disk system in deformed positions.

$$T = \frac{1}{2}\int_0^{\mathrm{l}} [m_s(\dot{U}_S^2 + \dot{V}_S^2) + \omega_R^2 I_{PS} + I_{dS}((\dot{U}_S')^2 + (\dot{V}_S')^2)]\,\mathrm{d}Z$$

$$+ \frac{1}{2}\int_0^{\mathrm{l}} [\omega_R I_{PS}(\dot{U}_S' V_S' - U_S' \dot{V}_S')]\,\mathrm{d}Z$$

$$+ \frac{1}{2}[M_d(\dot{U}_d^2 + \dot{V}_d^2) + \omega_R^2 I_{Pd} + I_{dd}((\dot{U}_d')^2 + (\dot{V}_d')^2)] + \frac{1}{2}[\omega_R I_{Pd}(\dot{U}_d' V_d' - U_d' \dot{V}_d')] \tag{3a}$$

$$U = \frac{EI}{2}\int_0^{\mathrm{l}} \{(U_S'')^2 + (V_S'')^2\}\,\mathrm{d}Z, \qquad D = \frac{1}{2}\int_0^{l} [C_T(\dot{U}_S^2 + \dot{V}_S^2) + C_R((\dot{U}_S')^2 + (\dot{V}_S')^2)]\,\mathrm{d}Z, \tag{4, 5}$$

$$W_e = (W_e)_P + (W_e)_T, \qquad (W_e)_P = \frac{1}{2}\int_0^{\mathrm{l}} ((U_S')^2 + (V_S')^2)\,\mathrm{d}Z - P(U_d' U_d + V_d' V_d)\,\mathrm{d}Z, \tag{6a}$$

$$(W_e)_T = T\int_0^{l} \{(V_d' - V_S')U_S'' - (U_d' - U_S')V_S''\}\,\mathrm{d}Z, \qquad P = P_0 \cos \omega_E t;$$

$$T = T_0 \cos \omega_E t, \tag{6b}$$

where C_T and C_R are the damping force and moment per unit length of the shaft, taken the same in all directions. P and T are the follower periodic axial force and torque loads. The subscripts d and S mean the quantities are referred to the disk and shaft, respectively. Since the shaft has a circular cross-section, it's polar moment of inertia is twice it's diametral moment of inertia, and this applies also to the disk.

The free vibration mode shapes of the non-rotating flexible shaft (without the disk) are used as the admissible functions in the assumed mode method to describe the vibratory motion of the rotating, deformed, and loaded shaft–disk system. Flexible deformations of the shaft, and the associated with them rigid disk translations and rotations are expressed below in terms of the non-rotating cantilever shaft mode shapes $\phi_n(Z)$ and the time dependent generalised co-ordinates $a_n(t)$ and $b_n(t)$:

$$U_S(Z, t) = \sum \phi_n(Z) a_n(t), \qquad V_S(Z, t) = \sum \phi_n(Z) b_n(t). \tag{7}$$

$$U_d(t) = U_S(Z = \ell, t) = \sum \phi_n(Z = \ell) a_n(t), \qquad V_d(t) = V_S(Z = \ell, t) = \sum \phi_n(Z = l) b_n(t). \tag{8}$$

$$\theta_{SX}(Z, t) = \frac{\partial V_S(Z, t)}{\partial Z} = \sum \phi_n'(Z) b_n(t), \qquad \theta_{SY}(Z, t) = \frac{\partial U_S(Z, t)}{\partial Z} = \sum \phi_n'(Z) a_n(t), \tag{9}$$

$$\theta_{dX}(Z, t) = \frac{\partial V_S(Z = \ell, t)}{\partial Z} = \sum \phi_n'(Z = \ell) b_n(t),$$

$$\theta_{dY}(Z, t) = \frac{\partial U_S(Z = \ell, t)}{\partial Z} = \sum \phi_n'(Z = \ell) a_n(t). \tag{10}$$

The uncoupled free vibration modes ϕ_n used as trial functions, are identical along the two principal directions due to the polar symmetry of the cross-section of the shaft under consideration. If the modal descriptions given above are substituted in the expressions for T, U, D, and W_e, the continuous system is replaced by a discrete system of an order equal to the total number of generalised co-ordinates $a_n(t)$ and $b_n(t)$, a form suitable for the application of Lagrange's equation

$$(\mathrm{d}/\mathrm{d}t)(\partial T/\partial \dot{q}_m) - (\partial T/\partial q_m) + (\partial U/\partial q_m) + (\partial D/\partial \dot{q}_m) = Q_m, \tag{11}$$

where $Q_m = \partial W_e/\partial q_m$ is the mth generalised force, resulting from the periodic non-conservative axial force P and end torque T; q_m can be any of the generalised co-ordinates a_n or b_n. Application of Lagrange's equation results in the following set of equations of motion:

$$\left\{\int_0^l [m_s \phi_m \phi_n + I_{dS} \phi_m' \phi_n'] \,\mathrm{d}Z + M_d \phi_m(\ell)\phi_n(\ell) + I_{dd} \phi_m'(\ell)\phi_n'(\ell)\right\}\ddot{a}_n$$

$$+ \left\{\int_0^l [C_T \phi_m \phi_n + C_R \phi_m' \phi_n'] \,\mathrm{d}Z\right\}\dot{a}_n + \omega_R \left\{\int_0^l I_{PS} \phi_m' \phi_n' \,\mathrm{d}Z + I_{Pd} \phi_m'(\ell)\phi_n'(\ell)\right\}\dot{b}_n$$

$$+ \left\{\int_0^l EI\phi_m'' \phi_n'' \,\mathrm{d}Z + P\left\{\phi_m(\ell)\phi_n'(\ell) - \int_0^l \phi_m' \phi_n' \,\mathrm{d}Z\right\}\right\}a_n$$

$$+ T\left\{\int_0^l \phi_m'' \phi_n' \,\mathrm{d}Z - \phi_n'(\ell)\int_0^l \phi_m'' \,\mathrm{d}Z\right\}b_n = 0, \qquad (m, n = 1, \ldots, N), \tag{12}$$

$$\left\{\int_0^l [m_s \phi_m \phi_n + I_{dS} \phi_m' \phi_n'] \,\mathrm{d}Z + M_d \phi_m(\ell)\phi_n(\ell) + I_{dd} \phi_m'(\ell)\phi_n'(\ell)\right\}\ddot{b}_n$$

$$+ \left\{\int_0^l [C_T \phi_m \phi_n + C_R \phi_m' \phi_n'] \,\mathrm{d}Z\right\}\dot{b}_n + \omega_R \left\{\int_0^l I_{ps} \phi_m' \phi_n' \,\mathrm{d}Z + I_{pd} \phi_m'(\ell)\phi_n'(\ell)\right\}\dot{a}_n$$

$$+ \left\{\int_0^l EI\phi_m'' \phi_n'' \,\mathrm{d}Z + P\left\{\phi_m(\ell)\phi_n'(\ell) - \int_0^l \phi_m' \phi_n' \,\mathrm{d}Z\right\}\right\}b_n$$

$$- T\left\{\int_0^l \phi_m'' \phi_n' \,\mathrm{d}Z - \phi_n'(l)\int_0^l \phi_m'' \,\mathrm{d}Z\right\}a_n = 0, \qquad (m, n = 1, \ldots, N). \tag{13}$$

Introducing the non-dimensional parameters

$$\mu = M_d/m_s\ell, \qquad k_s = \sqrt{I_{ds}/m_s\ell^2}, \qquad k_d = \sqrt{I_{dd}/M_d\ell^2}, \qquad \beta = P_0/P_{cr},$$
$$\gamma = T_0\ell/EI, \qquad B_T = C_T\ell^2/\sqrt{EIm_S}, \qquad B_R = C_R/\sqrt{EIm_S}, \qquad \eta = Z/\ell,$$
$$\tau = \omega_0 t, \qquad \Omega_E = \omega_E/\omega_0, \qquad \Omega_R = \frac{\omega_R}{\omega_0}, \qquad \omega_0 = \sqrt{EI/m_s\ell^4}$$

reduces the above equations to another set of more general and convenient-to-use non-dimensional equations of motion, given in matrix form:

$$[M]\{\overset{**}{X}\} + [C]\{\overset{**}{X}\} + [K]\{X\} = \{0\}, \tag{14}$$

where

P_{cr} is the Euler (critical) buckling load for the cantilever beam,

$$[\mathbf{M}] = \begin{bmatrix} [\mathbf{M}] & [\mathbf{0}] \\ [\mathbf{0}] & [\mathbf{M}] \end{bmatrix}, \qquad [\mathbf{C}] = \begin{bmatrix} [\mathbf{C}]_d & [\mathbf{C}]_g \\ -[\mathbf{C}]_g & [\mathbf{C}]_d \end{bmatrix}, \qquad [\mathbf{K}] = \begin{bmatrix} [\mathbf{H}] & [\mathbf{G}] \\ -[\mathbf{G}] & [\mathbf{H}] \end{bmatrix},$$

$$\{\mathbf{X}\} = [a_i\, b_i]^{\mathrm{T}},$$

$$M_{mn} = \int_0^1 [\phi_m \phi_n + k_s^2 \phi_m' \phi_n']\, \mathrm{d}\eta + \mu\{\phi_m(1)\phi_n(1) + k_d^2 \phi_m'(1)\phi_n'(1)\},$$

$$(C_{mn})_d = \int_0^1 [B_T \phi_m \phi_n + B_R \phi_m' \phi_n']\, \mathrm{d}\eta,$$

$$(C_{mn})_g = 2\Omega_R \left\{ \int_0^1 k_s^2 \phi_m' \phi_n'\, \mathrm{d}\eta + \mu k_d^2 \phi_m'(1)\phi_n'(1) \right\},$$

$$H_{mn} = \int_0^1 \phi_m'' \phi_n''\, \mathrm{d}\eta + \beta \cos \omega_E t \left\{ \phi_m(1)\phi_n'(1) - \int_0^1 \phi_m' \phi_n'\, \mathrm{d}\eta \right\},$$

$$G_{mn} = \gamma \cos \omega_E t \left\{ \int_0^1 \phi_m'' \phi_n'\, \mathrm{d}\eta - \phi_n'(1) \int_0^1 \phi_m''\, \mathrm{d}\eta \right\}.$$

Symbols $\{*\}$ and $()'$ denote differentiation with respect to non-dimensional time τ and spanwise co-ordinate η, respectively.

2.2. STABILITY ANALYSIS

To conduct the desired stability analyses, one first reduces the system with n second order equations to a system with $2n$ first order equations:

$$\{\dot{q}(\tau)\} = [A(\tau)]\{q(\tau)\},$$

where

$$\{q\} = \begin{Bmatrix} \dot{X} \\ X \end{Bmatrix}, \qquad [A] = \begin{bmatrix} [M]^{-1}[C] & [M]^{-1}[K] \\ [I] & [0] \end{bmatrix}$$

and $[A]$ is a periodic matrix with a common period T. The transition matrix $[\Phi(T, 0)]$ at the end of one period is calculated, and the stability of the system is determined by the characteristic exponents $\boldsymbol{\lambda}_k$, $k = 1, 2, \ldots, 2n$, which are related to the eigenvalues $\boldsymbol{\Lambda}_k$, $k = 1, 2, \ldots, 2n$, of the transition matrix by the relation $\mathrm{e}^{\lambda_k} = \boldsymbol{\Lambda}_k$, where $\boldsymbol{\lambda}_k$ and $\boldsymbol{\Lambda}_k$ are complex quantities in general, i.e., $\boldsymbol{\lambda}_k = \boldsymbol{\xi}_k + \mathrm{i}\omega_k$ and $\boldsymbol{\Lambda}_k = \boldsymbol{\Lambda}_{RK} + \mathrm{i}\boldsymbol{\Lambda}_{IK}$. It follows that $\xi_k = (1/2T) \ln (\boldsymbol{\Lambda}_{Rk}^2 + \boldsymbol{\Lambda}_{Ik}^2)$ and $\omega_k = (1/T) \tan^{-1} (\boldsymbol{\Lambda}_{Ik} / \boldsymbol{\Lambda}_{Ik})$. Since the real part of the characteristic exponent is a measure of growth or decay of the solution, then the system

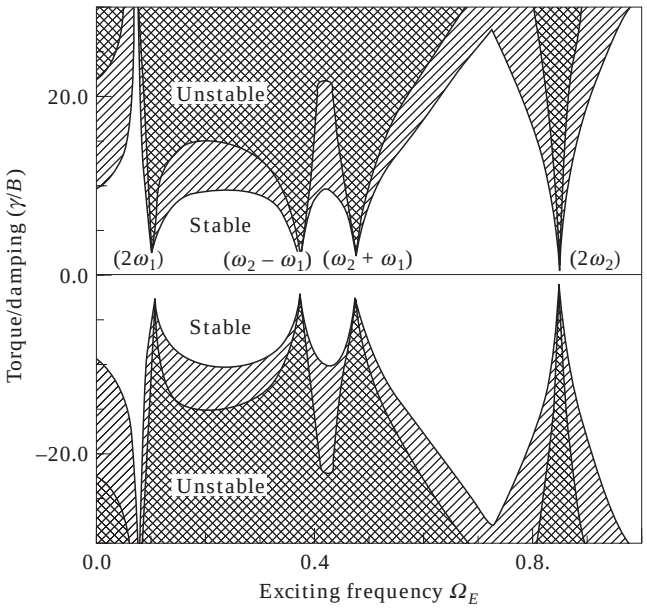

Figure 2. Stability boundaries in terms of torque-to-damping ratio versus the exciting frequency for $\beta/\gamma = 2{\cdot}0$ and $\Omega_R = 0{\cdot}0$. (▨, $B_R = 0{\cdot}0$ and $B_T = 0{\cdot}01$; ▩, $B_R = 0{\cdot}01$ and $B_T = 0{\cdot}0$).

will be unstable if the real part of any one of the characteristic exponents is greater than zero, i.e., $\xi_k > 0{\cdot}0$, or $|\Lambda_k| > 1{\cdot}0$.

3. RESULTS AND DISCUSSION

The stability boundaries are calculated for a flexible shaft–rigid disk system with $\mu = 10$, $k_S = 0{\cdot}1$, and $k_d = 0{\cdot}25$, and subjected to a periodic follower axial force $\beta \cos \omega_E t$ and end torque $\gamma \cos \omega_E t$. A computer program was developed to calculate the transition matrix $[\mathbf{\Phi}(T, 0)]$ at the end of one period. The real parts of the characteristic exponent ξ_k, which are a measure of system stability, were calculated from the eigenvalues of the transition matrix. The computer program was tested for the simple case with periodic follower axial force only. When an acceptable agreement between the calculated stability boundaries and those reported by Takahashi [16] was achieved, the more general case was considered, and the effect of axial force to end torque β/γ, end torque to damping ratio γ/B, and rotational speed Ω_R was evaluated, and the corresponding stability boundaries were presented.

In Figures 2 and 3, the calculated stability boundaries at rotor speeds $\Omega_R = 0{\cdot}0$ and $4{\cdot}0$, respectively, are presented in terms of the torque to damping ratio γ/B versus the exciting frequency Ω_E for the axial force to end torque ratio $\beta/\gamma = 2{\cdot}0$. It is necessary to mention here that in this study, the exciting frequency Ω_E is considered to be the same for both the axial force and end torque. The stability boundaries presented in Figures 2 and 3 cover positive and negative torque loads, which are found to respond differently to the gyroscopic moment associated with rotor speed. That is why the stability plots in Figure 3 are not symmetric with respect to the axis of zero torque, while the stability boundaries presented in Figure 2 are symmetric with respect to the same axis, because the latter were calculated for zero rotor speed, which implies zero gyroscopic moment. To examine the effect of the ratio of the axial force to the end torque β/γ, stability boundaries are

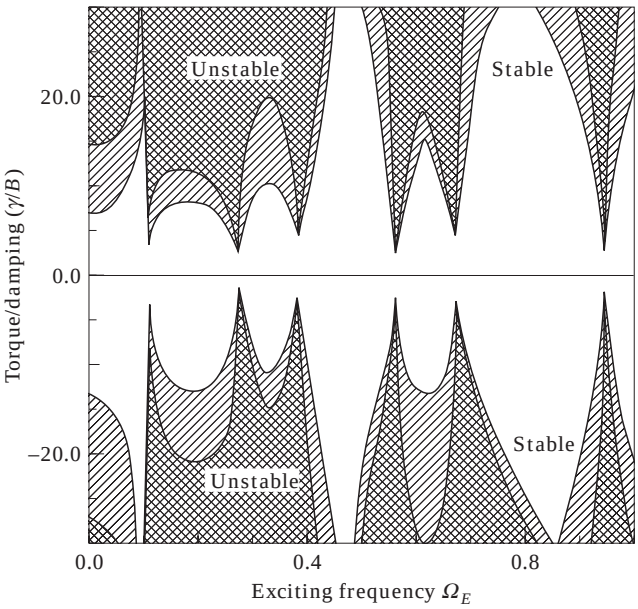

Figure 3. Stability boundaries in terms of torque-to-damping ratio versus the exciting frequency for $\beta/\gamma = 2{\cdot}0$ and $\Omega_R = 4{\cdot}0$. Key as for Figure 2.

calculated for given end torque to damping ratio γ/B and presented in terms of β/γ versus the exciting frequency Ω_E in Figures 4 and 5, for rotor speeds $\Omega_R = 0{\cdot}0$ and $4{\cdot}0$, respectively.

Two curves are shown in each of Figures 2–5. The first one with the wider unstable region was obtained with only translational damping accounted for, i.e., $B_R = 0{\cdot}0$ and $B_T = 0{\cdot}01$, and the second curve, with the smaller unstable region, was obtained with

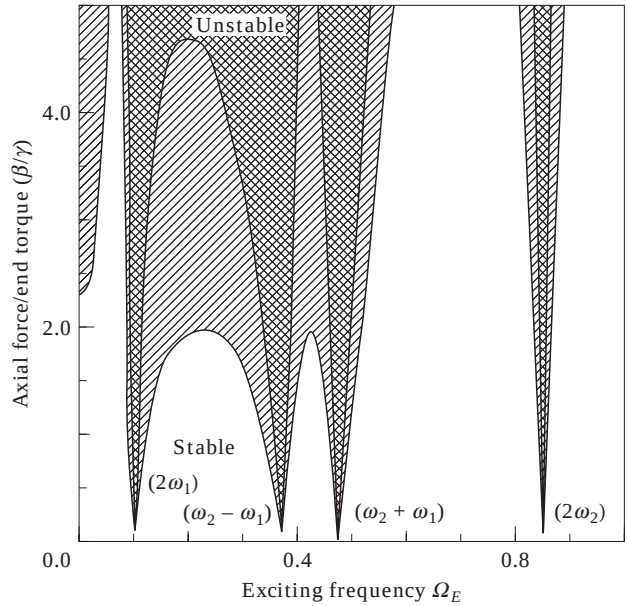

Figure 4. Stability boundaries in terms of torque-to-damping ratio versus the exciting frequency for $\gamma/B = 10{\cdot}0$ and $\Omega_R = 0{\cdot}0$. Key as for Figure 2.

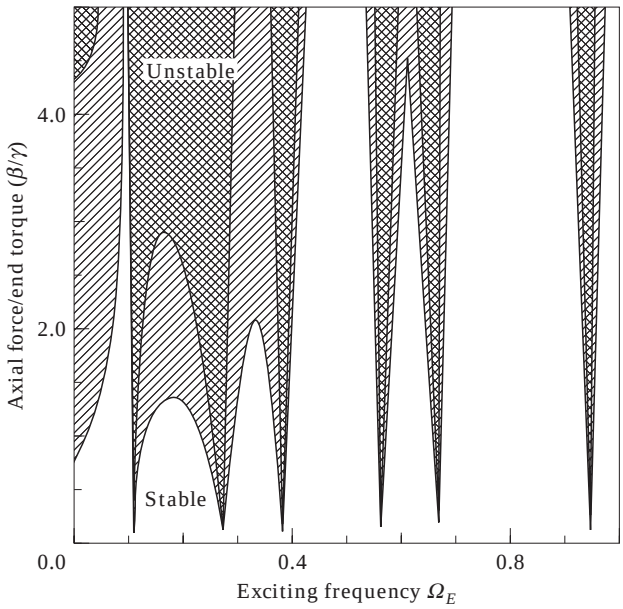

Figure 5. Stability boundaries in terms of axial force-to-end torque versus the exciting frequency for $\gamma/B = 10{\cdot}0$ and $\Omega_R = 4{\cdot}0$. Key as for Figure 2.

only the rotational damping accounted, for i.e., $B_R = 0{\cdot}01$ and $B_T = 0{\cdot}0$. This implies that the rotational damping B_R has a stronger stabilizing effect than the translational damping B_T. To further clarify the difference in the stabilizing effect due to B_T and B_R, calculations were carried out for shaft–disk system with $\beta/\gamma = 2{\cdot}0$ and $B_T = 0{\cdot}01$, and the stability boundaries obtained were presented in terms of the rotational to translational damping

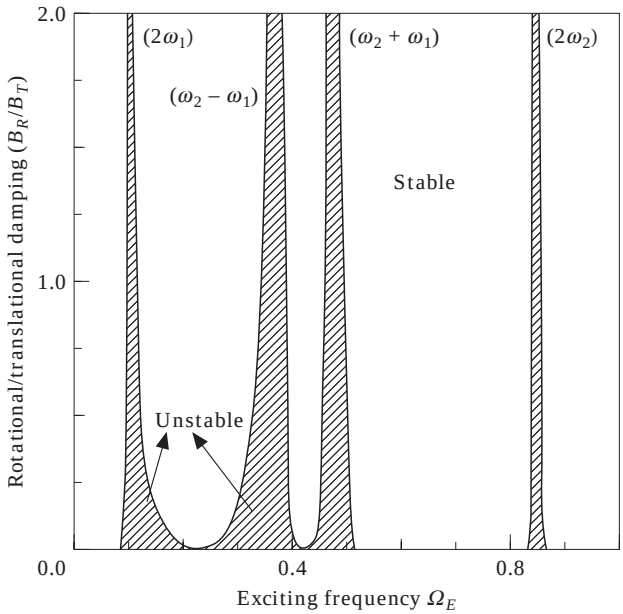

Figure 6. Stability boundaries in terms of rotational-to-translational damping versus the exciting frequency for $\beta/\gamma = 2{\cdot}0$ and $\Omega_R = 0{\cdot}0$.

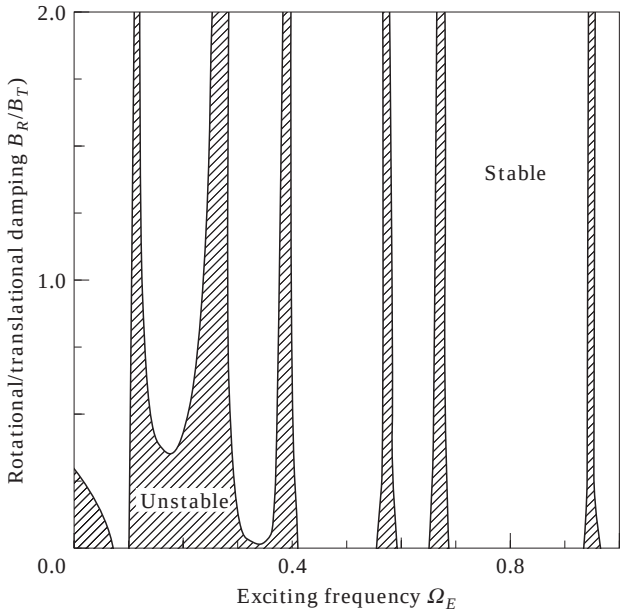

Figure 7. Stability boundaries in terms of rotational-to-translational damping versus the exciting frequency for $\beta/\gamma = 2{\cdot}0$ and $\Omega_R = 4{\cdot}0$.

ratio B_R/B_T versus the exciting frequency Ω_E in Figures 6 and 7, for rotor speeds $\Omega_R = 0{\cdot}0$ and $4{\cdot}0$, respectively. Similar calculations were made, but with $B_R = 0{\cdot}01$, and the obtained stability boundaries were presented in terms of the translational to rotational damping ratio B_T/B_R versus the exciting frequency Ω_E in Figures 8 and 9, for rotor speeds $\Omega_R = 0{\cdot}0$

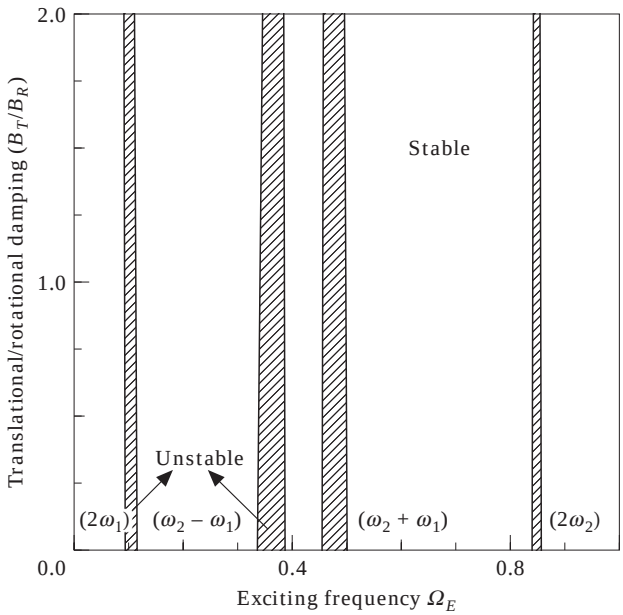

Figure 8. Stability boundaries in terms of translational-to-rotational damping versus the exciting frequency for $\beta/\gamma = 2{\cdot}0$ and $\Omega_R = 0{\cdot}0$.

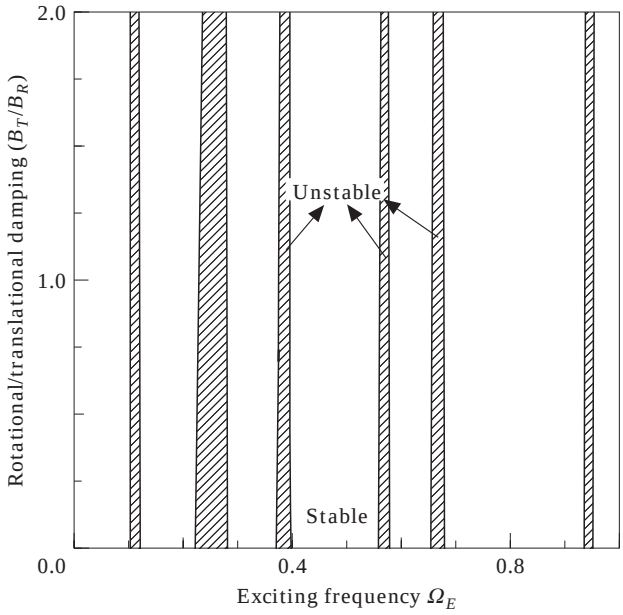

Figure 9. Stability boundaries in terms of translational-to-rotational damping versus the exciting frequency for $\beta/\gamma = 2{\cdot}0$ and $\Omega_R = 4{\cdot}0$.

and 4·0, respectively. From Figures 6 and 7, one notices that when B_R is increased from zero to twice the magnitude of B_T, a noticeable stabilizing effect is introduced and the unstable regions are reduced as B_R is increased. However, a much less stabilizing effect is noticed in Figures 8 and 9 as the translational damping B_T is increased from zero to twice the value of the rotational damping B_R, with other system parameters kept constant in

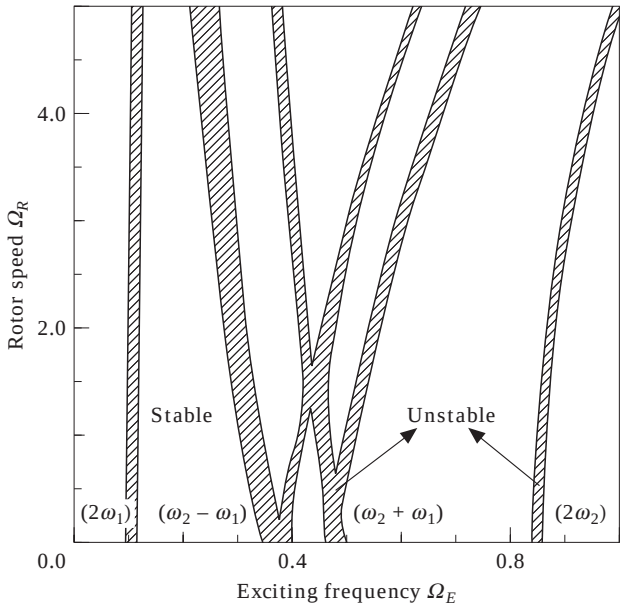

Figure 10. Stability boundaries in terms of rotor speed versus the exciting frequency.

both cases. This confirms the observation made from Figures 2–5, that the rotational damping B_R has a stronger stabilizing effect than the translational damping B_T.

As the frequency of the shaft–disk system splits during rotation into two frequencies, forward and backward, a similar split might take place in the calculated unstable regions. Such a split is noticed when Figures 3, 5, 7, and 9, on one hand, are compared with Figures 2, 4, 6, and 8 on the other hand, respectively. One has to remember that the former and latter sets of figures correspond to rotating and non-rotating systems, respectively. This is clearly illustrated in Figure 10, where the calculated stability boundaries for a shaft–disk system with $\beta/\gamma = 2{\cdot}0$, and $\gamma/B_R = \gamma/B_T = 10{\cdot}0$ are presented in terms of rotor speed Ω_R versus the exciting frequency Ω_E.

4. CONCLUSIONS

The governing equations of motion are derived for a rotating flexible shaft–rigid disk system, subjected to a periodic follower axial force and end torque. The equations obtained include periodic coefficients, and Floquet theory is used in the stability analyses. An efficient numerical integration scheme is employed to calculate the transition matrix at the end of one period. The method employed covers all types of instabilities without using the concept of small parameters and with no restriction on the parameters which affect system stability. The results presented provide designers with information about the performance of their product and allow them to select various design parameters to achieve the desired performance of their product. Examining the results presented, one concludes the following: first, the gyroscopic moment associated with rotor speed and moment of inertia interacts differently with positive and negative applied torque loads, which suggests that the correct sign of end torque is essential to obtain the correct stability boundaries. Second, the rotational damping in the system has a stronger stabilizing effect than the translational damping, and this is true for both positive and negative torque loads.

REFERENCES

1. R. G. Loewy and V. J. Piarulli 1969 *Dynamics of Rotating Shafts*. Washington, D.C.: The Shock and Vibration Information Center, United States Department of Defence.
2. Yukio Ishida, Takashi Ikeda, Toshio Yamamoto and Toshinori Esaka 1988 *JSME International Journal*, *Series III* **31**, 698–704. Parametrically excited oscillations of rotating shaft under a periodic axial force.
3. R. C. Kar and T. Sujata 1991 *Computers and Structures* **40**, 53–773. Dynamic stability of a rotating beam with various boundary conditions.
4. L.-W. Chen and D.-M. Ku 1992 *Transactions of the ASME*, *Journal of Vibration and Acoustics* **14**, 326–329. Dynamic stability of a cantilever shaft–disk system.
5. S. K. Sinha 1989 *AIAA Journal* **27**, 1653–1655. Stability of a viscoelastic rotor–disk system under dynamic axial loads.
6. S. K. Sinha 1989 *Journal of Sound and Vibrations* **131**, 509–514. Dynamic stability of a Timoshenko beam subjected to an oscillating axial force.
7. N. S. Namachchivaya 1998 *Journal of Sound and Vibrations* **133**, 323–336. Mean square stability of a rotating shaft under combined harmonic and stochastic excitations.
8. N. Khader 1995 *Journal of Sound and Vibrations* **182**, 759–773. Stability of rotating shafts loaded by follower axial force and torque load.
9. N. Willems and S. M. Holzer 1967 *Transactions of the ASME Journal of Engineering for Industry* **89**, 259–264. Critical speeds of rotating shafts subjected to axial loading and tangential torsion.
10. J. M. Vance 1978 *Transactions of the ASME Journal of Engineering for Industry* **100**, 235–240. A theory to explain non-synchronous whirling failure of rotors with high load torque.

11. J. M. Vance, K. B. Yim and S. T. Noah 1985 *Proceedings of the Symposium on Instability in Rotating Machinery*, Carson City, New York. Experimental verification and practical application of the torque whirl theory of rotor dynamic instability.
12. K. B. Yim, S. T. Noah and J. M. Vance 1986 *Transactions of the ASME, Journal of Applied Mechanics* **53**, 711–718. Effect of tangential torque on the dynamics of flexible rotors.
13. R. Cohen and I. Porat 1984 *Journal of Sound and Vibration* **95**, 151–160. Influence of load torque on stability of rotor driven by flexible shafts.
14. T. Aida and N. Ogawa 1993 *Journal of Sound and Vibration* **160**, 7–23. Dynamic stability of thin-walled structural members subjected to periodic axial follower torque and force.
15. F. Friedmann and C. E. Hammond 1977 *International Journal for Numerical Methods in Engineering* **11**, 1117–1136. Efficient numerical treatment of periodic systems with application to stability problems.
16. K. Takahashi 1981 *Journal of Sound and Vibration* **78**, 519–529. An approach to investigate the instability of the multiple-degree-of-freedom parametric dynamic systems.